EDEM-Based Performance Analysis and Parameter Optimization of an Integrated Soil Sampling and Sieving Device

Haiyuan Wang, Yunbo Peng, Shusong Wang, Peng Wang*

Longmen Laboratory, Luoyang, Henan, China

*Corresponding author email: wangp2024@126.com

Abstract. This study investigates an integrated soil sampling-sieving device using the EDEM discrete element method (DEM) to improve the efficiency of conventional separate sampling and sieving operations while reducing sample disturbance. The effects of auger rotational speed, descent speed, vibrating screen frequency, and screen inclination angle were evaluated through single-factor experiments and a Box-Behnken design (BBD). Second-order response surface models were established for sample recovery rate (RR), sieving efficiency (Et), and blockage rate (B). The RR, Et, and B models were highly significant ($p<0.01$), with coefficients of determination of 0.9505, 0.835, and 0.833, respectively, while the disturbance index (Dr) remained stable at 20.23%-21.33%, indicating low sensitivity to the tested operating parameters. Multi-objective optimization identified the optimal parameter combination as 649 rpm rotational speed, 0.06 m/s descent speed, 20Hz vibration frequency, and 12 degrees screen inclination. The predicted responses were RR=70.57%, Dr=20.41%, Et=35.27%, and B=12.65%. Three replicate DEM validation simulations produced relative errors of 0.07%-0.45%. Physical validation with a simplified prototype further confirmed the optimized parameters, with relative errors below 7% for RR, Et, and B, demonstrating reasonable agreement between simulation and field results.

Keywords: soil sampling; sieving device; EDEM; discrete element method; Box-Behnken design; parameter optimization

1 Introduction

Soil sampling is a fundamental task in geotechnical engineering investigation, agricultural soil survey, and environmental monitoring. The quality of soil samples directly affects the reliability of subsequent geotechnical test results and the scientific validity of engineering decisions. In conventional workflows, soil sampling and sieving are typically conducted as two independent stages: samples are collected in the field and then transported to a laboratory for sieving. This process is not only inefficient but also introduces additional errors, as vibration and disturbance during transportation can alter the particle size distribution and structural characteristics of the soil samples. Therefore,

© The Author(s) 2026
L. L. Kuan et al. (eds.), *Proceedings of the 2026 3rd International Symposium on Agricultural Engineering and Biology (ISAEB 2026)*, Advances in Biological Sciences Research 56,
https://doi.org/10.2991/978-94-6239-847-4_22

integrating sampling and sieving functions into a single device presents a clear engineering demand.

Since its inception by Cundall and Strack [1], the discrete element method (DEM) has been widely used to analyze soil-tool interactions and particle screening processes. Previous studies have optimized auger drilling, fertilizer injection, and vibrating screening devices using EDEM, response surface methodology, and intelligent optimization algorithms [2-5]. These studies provide useful references for parameter calibration and single-function device optimization. However, most existing work focuses on either sampling or sieving alone, while the coupled effects of auger speed, descent speed, vibration frequency, and screen inclination in an integrated sampling-sieving device remain unclear.

This paper takes an integrated soil sampling-sieving device as the research object. Based on the EDEM simulation platform, a combination of single-factor experiments and Box-Behnken design (BBD) is employed to systematically investigate the effects of auger rotational speed, descent speed, vibrating screen frequency, and screen inclination angle on sample recovery rate, disturbance index, sieving efficiency, and blockage rate. Multi-response prediction models are established and multi-objective optimization is performed, aiming to provide quantitative guidance for the design and operation of integrated soil processing devices.

2 Materials and Methods

2.1 Soil Parameters and DEM Model Calibration

The sandy soil used in this study was collected from the plough layer (0-30 cm depth) at Changqinglin, Hua County, Anyang City, Henan Province, China (114°35′0.208″E, 35°36′43.945″N). The measured average wet density was 1.36 g/cm3, dry density 1.34 g/cm3, and moisture content 1.74%. Particle size distribution was gravel (>1-2 mm) 1.25%, sand (0.075-1 mm) 90.09%, and silt (<0.075 mm) 8.66%. The internal friction angle was 34.8°, and Poisson ratio was 0.30, determined following standard soil testing procedures for DEM parameter calibration [6]. The physical parameters of the materials used in the DEM model are listed in Table 1.

Given the low moisture content and negligible inter-particle cohesion, the Hertz-Mindlin (no slip) contact model was selected. Soil particles were simplified into five common shapes using a multi-sphere combination method: single sphere, double sphere, triple sphere, four-square sphere, and linear four-sphere, with particle sizes ranging from 0.075 to 1 mm. To balance computational efficiency and simulation accuracy, particle sizes and geometric models were scaled up by a factor of three.

The natural angle of repose was measured using the funnel method and used as the calibration benchmark for DEM contact parameters [7,8]. Five physical replicates gave an average repose angle of 37.59°. The physical and simulated soil accumulation profiles are compared in Figure 1. A mixed-level full factorial design was then conducted for the soil-soil restitution coefficient, static friction coefficient, and rolling friction coefficient, producing 18 parameter combinations. The simulated repose angles ranged from 35.59° to 46.81°, covering the measured value. The optimal parameter set was

determined as a restitution coefficient of 0.75, static friction coefficient of 0.85, and rolling friction coefficient of 0.25, with a simulated repose angle of 37.56° and a relative error of 0.1%. Therefore, this calibrated parameter set was adopted in subsequent DEM simulations. The contact parameters used in the subsequent DEM simulations are summarized in Table 2.



(a) Physical test (b) Simulation test

Fig. 1. Comparison between physical test and simulation test of soil accumulation

Table 1. Material physical parameters

Material	Poisson's ratio	Density (kg/m3)	Shear modulus (Pa)
Soil	0.30	1360	1x10^8
65Mn steel	0.35	7830	7.27x10^10

Table 2. Contact parameters

Contact pair	Static friction	Rolling friction	Restitution
Soil-Soil	0.85	0.25	0.75
Soil-65Mn steel	0.31	0.10	0.50

2.2 Device Model and Simulation Setup

Three-dimensional solid models of the auger sampling device and vibrating sieving device were constructed at a 1:1 scale, with non-essential components such as mounting brackets and fasteners removed to reduce computational load, as shown in Figure 2. The auger was a double-flight spiral drill with an outer diameter of 60 mm, a core diameter of 20 mm, a total length of 800 mm, and an effective working length of 550 mm. The sleeve had an inner diameter of 62 mm, leaving a 1 mm clearance around the auger, and a discharge port was arranged at the top to convey the sampled soil to the vibrating screen. To balance computational efficiency and simulation fidelity, the soil particle size and screen aperture size were scaled up by a factor of three; therefore, the screen aperture diameter was set to 3 mm. The vibrating screen performed reciprocating vibration along the inclination direction with a fixed amplitude of 2 mm.

During simulation, the auger simultaneously rotates about its axis and feeds axially, with rotational speed ranging from 200 to 800 rpm, descent speed from 0.05 to 0.20 m/s, and fixed sampling depth of 400 mm. The screen inclination angle ranged from 5° to 20°, and the vibration frequency ranged from 10 to 40 Hz. The initial soil particle bed was generated using the gravity deposition method.

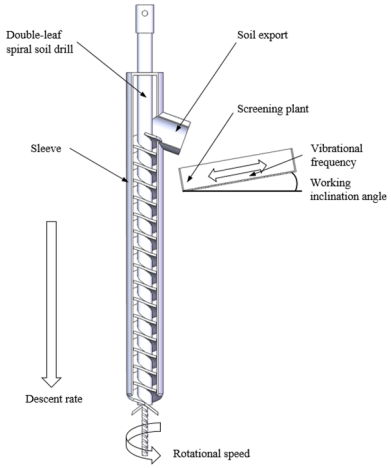


Fig. 2. Integrated soil sampling-sieving device

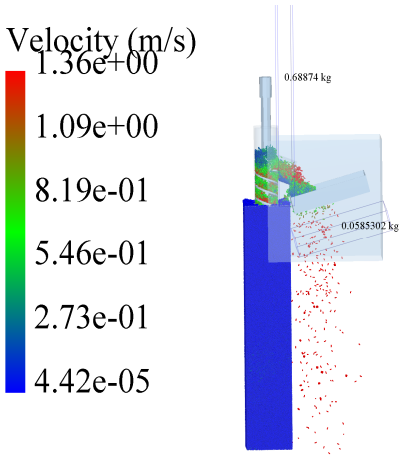


Fig. 3. DEM simulation model of the sampling-sieving process

2.3 Evaluation Indicators

Four quantitative indicators were selected to comprehensively evaluate device performance:

(1) Sample recovery rate (RR): the ratio of soil mass actually collected in the collection hopper to the theoretical sampling mass (approximately 1.35 kg, based on rho = 1360 kg/m3, drill diameter 0.06 m, sampling depth 0.35 m). Higher RR indicates better sampling efficiency.

(2) Disturbance index (Dr): the ratio of the standard deviation of marked particle displacement after sampling to the auger outer diameter. Marked particles were selected within a rectangular region (60 mm x 50 mm x 25 mm) located 20 mm from the drill axis. Lower Dr indicates higher sampling quality.

(3) Sieving efficiency (Et): the ratio of fine particle mass actually passing through the screen to the total fine particle mass in the feed. Higher Et indicates better sieving performance.

(4) Blockage rate (B): the ratio of blocked mesh holes to the total number of holes (221). A hole is considered blocked when all particles within it exhibit minimum vertical velocity (i.e., jammed and unable to pass). Lower B indicates smoother sieving operation.

3 Single-factor Experiments

To determine the influence trends and reasonable ranges of each operating parameter, 12 single-factor simulation experiments were conducted (6 for auger parameters, 6 for screen parameters). Each working condition was simulated once using the DEM simulation model shown in Figure 3. The results are summarized in Table 3.

Table 3. Single-factor experiment matrix and response values

No.	Factor	Level	Fixed condition	Response
S-1	Rotational speed	200 rpm	Descent 0.10 m/s	RR=12.50%,Dr=20.35%
S-2	Rotational speed	500 rpm	Descent 0.10 m/s	RR=63.74%,Dr=21.05%
S-3	Rotational speed	800 rpm	Descent 0.10 m/s	RR=70.94%,Dr=20.51%
S-4	Descent rate	0.05 m/s	Speed 800 rpm	RR=60.54%,Dr=21.20%
S-5	Descent rate	0.10 m/s	Speed 800 rpm	RR=70.94%,Dr=20.51%
S-6	Descent rate	0.20 m/s	Speed 800 rpm	RR=27.60%,Dr=20.30%
V-1	Frequency	10 Hz	Angle 10 deg	Et=3.34%, B=76.47%
V-2	Frequency	20 Hz	Angle 10 deg	Et=31.54%, B=14.90%
V-3	Frequency	40 Hz	Angle 10 deg	Et=22.02%, B=28.96%
V-4	Angle	5 deg	Freq. 20 Hz	Et=47.83%, B=31.22%
V-5	Angle	10 deg	Freq. 20 Hz	Et=31.54%, B=14.90%
V-6	Angle	20 deg	Freq. 20 Hz	Et=16.62%, B=18.55%

The experimental results demonstrate the following trends. (1) Rotational speed: RR increases significantly with speed (12.50% at 200 rpm to 70.94% at 800 rpm), as low-speed results in insufficient blade linear velocity and limited chip removal capacity. Dr remains stable at 20.35%-21.05% across all speeds. (2) Descent speed: RR follows a rise-then-fall trend, peaking at 70.94% at 0.10 m/s and dropping sharply to 27.60% at 0.20 m/s due to chip congestion from overly rapid feeding. Dr remains stable at 20.30%-21.20%. (3) Vibration frequency: Et peaks at 31.54% (20 Hz) while B is minimized at 14.90% (20 Hz); low frequency causes insufficient vibration energy and severe blockage, while high frequency reduces the particle passing window. (4) Screen inclination: Et decreases monotonically with angle (47.83% at 5° to 16.62% at 20°), and B is lowest at 10° (14.90%).

In summary, RR is sensitive to rotational speed and descent speed; Et and B are sensitive to frequency and inclination; Dr is insensitive to all parameters (stable at 20.30%-21.20%). Based on these results, the BBD factor levels were set as: rotational speed 500/650/800 rpm, descent speed 0.05/0.10/0.15 m/s, frequency 20/30/40 Hz, and inclination 5°/10°/15°.

4 Box-Behnken Response Surface Optimization

4.1 Experimental Design

A four-factor three-level Box-Behnken design (BBD) was employed, comprising 27 experimental points (24 factorial points + 3 center point replicates). BBD is an efficient response surface methodology requiring fewer runs than central composite designs while effectively fitting second-order models [9]. The center point (A=650rpm, V=0.10m/s, C=30Hz, D=10°) was replicated three times to estimate pure error. These three center-point simulations were used to estimate pure error and evaluate the repeatability of the DEM simulation process under identical operating parameters. The experimental matrix and response values are presented in Table 4. The standard deviations of the center point replicates were 2.85% for RR, 0.26% for Dr, 0.22% for Et, and 1.23% for B, indicating good simulation repeatability.

Table 4. Box-Behnken experimental matrix and response values

Run	A(rpm)	V(m/s)	C(Hz)	D(deg)	RR (%)	Dr (%)	Et(%)	B (%)
1	500	0.05	30	10	66.11	20.68	20.59	26.70
2	800	0.05	30	10	48.75	20.56	32.63	28.05
3	500	0.15	30	10	49.00	21.26	22.36	14.03
4	800	0.15	30	10	36.42	20.73	36.20	16.74
5	650	0.10	20	5	45.30	20.60	40.79	16.74
6	650	0.10	40	5	47.27	20.68	21.87	31.22
7	650	0.10	20	15	60.75	21.33	23.96	20.36
8	650	0.10	40	15	59.13	21.31	9.46	24.43
9	500	0.10	20	10	63.74	21.05	24.98	13.12
10	800	0.10	20	10	64.46	20.51	31.54	14.90
11	500	0.10	40	10	65.31	20.97	12.86	24.89
12	800	0.10	40	10	56.61	20.70	22.02	28.96
13	650	0.05	30	5	46.98	20.41	30.06	28.05
14	650	0.15	30	5	42.31	21.20	28.06	27.15
15	650	0.05	30	15	67.29	20.41	19.06	25.33
16	650	0.15	30	15	46.04	20.32	12.48	13.12
17	500	0.10	30	5	43.35	20.97	25.89	24.89
18	800	0.10	30	5	46.71	20.33	29.72	32.58
19	500	0.10	30	15	58.64	20.53	12.66	20.81
20	800	0.10	30	15	45.49	20.67	15.63	23.98
21	650	0.05	20	10	49.62	20.42	33.05	18.10
22	650	0.15	20	10	32.51	21.15	33.51	30.78
23	650	0.05	40	10	72.52	20.67	15.09	34.84
24	650	0.15	40	10	43.80	20.61	14.09	29.86
25	650	0.10	30	10	44.25	21.14	19.65	28.96
26	650	0.10	30	10	43.42	20.23	26.71	30.32
27	650	0.10	30	10	48.78	20.74	26.76	28.51

Note: Experiments 25-27 are center-point repetitions (A=650 rpm, V=0.1 m/s, C=30 Hz, D=10°).

4.2 ANOVA and Regression Models

The regression analysis of the test data was conducted using the Design-Expert 13.0 software, and the second-order regression equations between rotational speed (A), descent speed (V), frequency (C), inclination angle (D) and sample recovery rate (RR), disturbance index (Dr), sieving efficiency (Et) and blockage rate (B) were obtained. Under the premise of ensuring the significant model, the final quadratic regression model equations for each evaluation index were obtained:

$$RR = 45.48 - 1.02A - 4.28V + 0.04C + 0.55D - 2.08AV + 4.82AC - 1.34AD - 3.61VC - 4.53VD - 0.71CD + 5.90A^2 + 11.08V^2 + 3.83C^2 - 4.91D^2 \quad (1)$$

$$Et = 24.37 + 0.99A - 1.04V - 4.39C - 1.30D + 2.51AV - 5.67AC - 5.56AD + 2.81VC - 2.24VD + 3.88CD + 7.17A^2 + 0.92V^2 - 4.87C^2 - 4.19D^2 \quad (2)$$

$$B = 29.26 + 0.81A + 1.91V - 1.77C - 0.14D + 0.10AV - 2.97AC + 2.53AD + 2.46VC - 6.01VD + 1.94CD - 3.92A^2 - 4.22V^2 - 4.35C^2 + 2.08D^2 \quad (3)$$

As shown in Table 5, the ANOVA results for the sample recovery rate (RR), sieving efficiency (Et), and blockage rate (B) models are all highly significant, indicating that the analysis results are valid. Among them, the descent speed V has a considerable effect on RR, the working frequency C has a considerable effect on Et, and B is significantly affected by both descent speed V and working frequency C. In addition, the p-value of the disturbance index (Dr) model is 0.4668, indicating that the model is not significant. The p-values of all factors and interaction terms exceed 0.05, with none reaching the significance level. Dr remains stable at 20.23%~21.33% across all 27 experiments (a range of 1.10 percentage points), confirming that the disturbance characteristic of the device is insensitive to operating parameters. Given the non-significant model, no further response surface analysis is conducted for Dr.

Table 5. Model variance analysis table

Source	RR		Et		B		Dr	
	F	p	F	p	F	p	F	p
Model	16.46	<0.0001**	4.34	0.0073**	4.28	0.0078**	1.06	0.4668
A	2.40	0.1467	0.82	0.3828	0.81	0.3866	-	-
V	33.23	<0.0001**	1.98	0.1845	4.92	0.0468*	-	-
C	0.01	0.9425	20.23	0.0007**	4.96	0.0459*	-	-
D	0.55	0.4713	0.97	0.3441	0.02	0.9000	-	-
AV	2.03	0.1796	1.36	0.2664	0.00	0.9588	-	-
AC	10.83	0.0064**	6.94	0.0218*	2.45	0.1431	-	-
AD	0.84	0.3778	6.67	0.0241*	1.79	0.2057	-	-
VC	6.07	0.0294*	1.70	0.2166	1.68	0.2190	-	-
VD	9.57	0.0091**	1.09	0.3179	10.05	0.0080**	-	-
CD	0.24	0.6352	3.26	0.0961	1.04	0.3270	-	-
A^2	18.83	0.0010**	12.85	0.0038**	4.99	0.0453*	-	-
V^2	64.77	<0.0001**	0.20	0.6616	5.61	0.0354*	-	-
C^2	7.74	0.0165*	5.79	0.0330*	5.95	0.0313*	-	-
D^2	12.73	0.0038**	4.28	0.0608	1.36	0.2658	-	-
Lack of fit	1.13	0.1806	1.05	0.1199	1.84	0.0550	0.87	0.5416

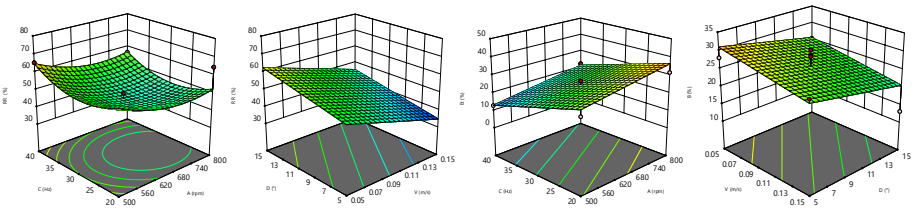
Note: ** indicates a highly significant effect ($p < 0.01$), and * indicates a significant effect ($0.01 <= p < 0.05$).

4.3 Interaction Analysis

The response surfaces for the significant factor interactions were plotted using Design-Expert 13.0 software, as shown in Figure 4 (a)–(d). As illustrated in Figures 4(a) and 4(b), AC (rotational speed × frequency), VC (descent speed × frequency), and VD (descent speed × inclination angle) exert significant effects on RR. At low frequency (20 Hz), RR first increases and then decreases with rotational speed, reaching a peak of approximately 64% near 650 rpm; at high frequency (40 Hz), RR declines continuously with rotational speed—high-frequency vibration loosens the soil sample in the collection hopper and disrupts the continuity of auger chip discharge. At a large inclination angle (15°), RR decreases markedly with descent speed (from 67% to 46%), as the material slides rapidly across the screen surface and the feed rate exceeds the chip removal capacity.

Figure 4(c) depicts the response surface of Et as a function of rotational speed A and frequency C(with V=0.10m/s and D=10°). At low frequency, Et rises with increasing rotational speed (25%→32%). At high frequency, Et likewise increases with rotational speed (13%→22%), but remains approximately 10% lower overall. The adverse effect of rising frequency on Et is more pronounced at low rotational speed (12% reduction), whereas the reduction narrows to 10 percentage points at high rotational speed.

As indicated by the ANOVA results, VD (descent speed × inclination angle) has a highly significant effect on blockage rate B and is the dominant interaction term governing B. Figure 4(d) presents the response surface of B as a function of descent speed V and inclination angle D(with A= 650rpm and C=30Hz). At D= 5°, B decreases slightly with V(28.1%→27.2%). At D=15°, B decreases substantially with V(25.3%→13.1%), representing a reduction of 12.2%. A larger inclination angle thins the material bed and shortens residence time, making it less likely for particles to become lodged in the screen apertures.



(a) RR(A, C) (b) RR(D, V) (c)Et (d) B

Fig. 4. Response surface plots of significant factor interactions

4.4 Multi-objective Optimization and Validation

Multi-objective optimization was performed using the desirability function approach, which has been widely applied in agricultural machinery parameter optimization [9,10]. RR and Et were set as larger-the-better (weight 0.4 each), while Dr and B were set as smaller-the-better (weight 0.1 each). The optimal parameter combination and predicted response values are presented in Table 6.

Table 6. Optimal parameter combination and predicted responses

Parameter	Optimal value	Response	Predicted value
Speed A (rpm)	649	RR (%)	70.57
Descent V (m/s)	0.06	Dr (%)	20.41
Frequency C (Hz)	20	Et (%)	35.27
Inclination D (deg)	12	B (%)	12.65

Three replicate validation simulations were conducted using the optimal parameter combination. The relative error was calculated as the absolute difference between the predicted value and the mean value of the three validation simulations divided by the predicted value. The results are shown in Table 7. The relative errors for all response variables are below 1%, confirming good prediction accuracy of the response surface models and the reliability of the optimization results.

Table 7. Validation experiment results

Response	Predicted	Mean +/- SD	Rel. error (%)
RR (%)	70.57	70.52 +/- 1.01	0.07
Dr (%)	20.41	20.39 +/- 0.09	0.10
Et (%)	35.27	35.43 +/- 0.60	0.45
B (%)	12.65	12.60 +/- 0.37	0.40

Note: SD denotes the sample standard deviation of three replicate validation simulations (n = 3). The relative errors between the predicted and mean simulated values were 0.07%, 0.10%, 0.45%, and 0.40% for RR, Dr, Et, and B, respectively.

4.5 Physical Validation

To further validate the reliability of the optimized parameter combination obtained from the DEM simulations, a simplified prototype was fabricated and field-tested at the original soil sampling site. The prototype retained the core structural dimensions and kinematic functions of the simulated device, including the 60 mm auger diameter, the 3 mm screen aperture, and the adjustable vibration and inclination mechanisms. The soil conditions of the experimental site were similar to those described in Section 2.1, with a moisture content of 2.74% and a similar particle size distribution. This ensured the comparability between the field experiments and the DEM prediction results.

The integrated device mainly consists of a main frame, an auger sampling mechanism, a power unit, and a vibrating screen unit, as shown in Figure 5. The auger sampling mechanism lifts soil through the sleeve during the soil discharging process, and the discharged soil is then conveyed to the vibrating screen unit for the sieving process.



Fig. 5. Prototype Unit and Field Test

During each test, the prototype was operated under the optimal parameter combination (A = 649 rpm, V = 0.06 m/s, C = 20 Hz, D = 12°), following the same operational sequence as in the simulations. The soil mass collected in the sampling hopper and the mass passing through the vibrating screen were weighed using an electronic balance

(accuracy ±0.01 g) to calculate RR and Et, respectively. The number of blocked mesh holes was visually counted after each test to obtain B. Each test was replicated three times under identical conditions to ensure statistical reliability; the mean and standard deviation of each indicator were calculated.

The physical validation results are summarized in Table 8. The experimental values of RR, Et, and B were 66.50% ± 1.15%, 32.85% ± 0.95%, and 13.48% ± 0.42%, respectively. The relative errors between the physical experimental results and the DEM predictions were 5.77%, 6.86%, and 6.56% for RR, Et, and B, respectively. The discrepancies can be attributed to the simplified nature of the prototype, which may introduce additional mechanical clearances and edge effects not present in the idealized DEM model, as well as inherent variations in field soil conditions. Despite these minor deviations, the relative errors are within 7%, demonstrating reasonable agreement between simulation and experimental results and confirming the practical feasibility of the optimized parameters.

Table 8. Physical validation experiment results under the optimal parameter combination

Response	Predicted	Mean +/- SD	Rel. error (%)
RR (%)	70.57	66.50+/- 1.15	5.77
Et (%)	35.27	32.85+/- 0.95	6.86
B (%)	12.65	13.48+/-0.42	6.56

Note: SD denotes the sample standard deviation of three replicate field tests (n = 3). All tests were conducted under the optimal parameter combination (A = 649 rpm, V = 0.06 m/s, C = 20 Hz, D = 12°).

5 Conclusion

This study employed a combination of single-factor experiments and Box-Behnken design to systematically investigate the effects of auger rotational speed, descent speed, vibrating screen frequency, and screen inclination angle on the performance of an integrated soil sampling-sieving device. Response surface prediction models were established, and multi-objective optimization was performed. The main conclusions are as follows.

(1) Single-factor experiments showed that RR increases with rotational speed (12.50% to 70.94%) and follows a rise-then-fall trend with descent speed (optimal at 0.10 m/s). Et decreases with increasing frequency and inclination, while B is minimized at 20 Hz and 10°. Dr remains stable at 20.30%-21.20% across all conditions, insensitive to operating parameters.

(2) The BBD regression models for RR, Et, and B are all highly significant ($p < 0.01$) with R-squared values of 0.9505, 0.835, and 0.833, respectively. The validation related errors ranged from 0.07% to 0.45%, indicating good model prediction accuracy. The Dr model is not significant ($p = 0.4668$), with a range of only 1.10 percentage points across 27 experiments, further confirming its parameter insensitivity.

(3) ANOVA revealed key interaction effects: speed × frequency (AC) and descent × inclination (VD) significantly affect RR; AC and speed × inclination (AD) significantly

affects Et; VD is the most significant factor for B. These interaction terms provide quantitative guidance for parameter matching strategies.

(4) The optimal parameter combination was obtained by multi-objective optimization: speed 649 r/min, descent speed 0.06m/s, frequency 20Hz, inclination angle 12°. The predicted values were RR = 70.57 %, Dr = 20.41 %, Et = 35.27 %, B = 12.65 %. Three replicate DEM validation simulations under this combination yielded relative errors of 0.07%, 0.10%, 0.45%, and 0.40% for RR, Dr, Et, and B, respectively, confirming the good predictive accuracy of the response surface models. Physical validation experiments using a simplified prototype further verified the optimized parameters, with relative errors of 5.77%, 6.86%, and 6.56% for RR, Et, and B, respectively, all within 7%, demonstrating reasonable agreement and practical feasibility.

(5) For practical operation under the low-moisture sandy soil condition considered in this study, the recommended operating ranges are rotational speed of 600-700 rpm, descent speed of 0.05-0.08 m/s, vibration frequency of 20 Hz, and screen inclination of 10-12°. Combinations of low rotational speed (< 500 rpm) with high descent speed (> 0.12 m/s), and high vibration frequency (> 35 Hz) with small inclination angle (< 8°), should be avoided.

Future work will extend the validation to soils with varying moisture contents and textures to further evaluate the generalizability of the device under diverse field conditions.

Acknowledgement

This research was funded by Scientific and Technological Research Projects in Henan Province, grant number 252102110376; International Science and Technology Cooperation Project of Henan Province, grant number 262102520050; the Key Research and Development Special Project of Henan Province, grant number 241111114100; Heluo Youth Innovation and Entrepreneurship Talent Project in 2024; the Frontier Exploration Projects of Longmen Laboratory, grant number: LMQYQN202403. The authors gratefully acknowledge the experimental facilities provided by Longmen Laboratory.

Disclosure of Interests

The authors have no competing interests to declare that are relevant to the content of this article.

References

1. Cundall, P. A., Strack, O. D. L.: A discrete numerical model for granular assemblies. Géotechnique 30(3), 331–336 (1980). DOI: 10.1680/geot.1980.30.3.331.
2. Wang, G., Zhang, W., Ji, M., et al.: Numerical simulation and parameter optimization of earth auger in hilly area using EDEM software. Scientific Reports 12, 19526 (2022). DOI: 10.1038/s41598-022-23833-2.

3. Liu, H., Xu, W., Yuan, Q., et al.: Optimization and experimental study of operation parameters for fertilizer injection drilling device based on discrete element simulation. Applied Sciences 14, 2642 (2024). DOI: 10.3390/app14062642.
4. Li, Z., Tong, X., Zhou, B., et al.: Modeling and parameter optimization for the design of vibrating screens. Minerals Engineering 83, 149–155 (2015). DOI: 10.1016/j.mineng.2015.07.009.
5. Yang, J., Zhang, W., Gao, J., et al.: Optimizing RAP sieving efficiency of linear vibrating sieve using DEM simulation. Construction and Building Materials 333, 127442 (2022). DOI: 10.1016/j.conbuildmat.2022.127442.
6. Pang, J., Lin, X., Chen, S., et al.: Study on measurement and calibration methods of soil parameters used in discrete element method. Journal of Anhui Agricultural Sciences 51(18), 6–11 (2023). DOI: 10.3969/j.issn.0517-6611.2023.18.002.
7. Zhang, X., Zhang, L., Hu, X., et al.: Calibrating contact parameters of typical rotary tillage components cutting soil based on different simulation methods. Scientific Reports 13, 5757 (2023). DOI: 10.1038/s41598-023-32881-1.
8. Song, S., Tang, Z., Zheng, X., et al.: Calibration of the discrete element parameters for the soil model of cotton field after plowing in Xinjiang of China. Transactions of the Chinese Society of Agricultural Engineering 37(20), 63–70 (2021). (in Chinese with English abstract). DOI: 10.11975/j.issn.1002-6819.2021.20.007.
9. Shi, N., Li, H., Jiang, B., et al.: Design and parameter optimization of a vertical rotary fixed-angle straw cleaning device. Agriculture 15(20), 2113 (2025). DOI: 10.3390/agriculture15202113.
10. Xu, N., Yu, C., Gong, S., et al.: Numerical study and multi-objective optimization of flexible screening process of flip-flow screen: A DEM-FEM approach. Advanced Powder Technology 33(7), 103650 (2022). DOI: 10.1016/j.apt.2022.103650.

Open Access This chapter is licensed under the terms of the Creative Commons Attribution-NonCommercial 4.0 International License (http://creativecommons.org/licenses/by-nc/4.0/), which permits any noncommercial use, sharing, adaptation, distribution and reproduction in any medium or format, as long as you give appropriate credit to the original author(s) and the source, provide a link to the Creative Commons license and indicate if changes were made.

The images or other third party material in this chapter are included in the chapter's Creative Commons license, unless indicated otherwise in a credit line to the material. If material is not included in the chapter's Creative Commons license and your intended use is not permitted by statutory regulation or exceeds the permitted use, you will need to obtain permission directly from the copyright holder.

